

CHARACTERIZATION OF THE SOLVENT-INDUCED NONLINEAR RESPONSE OF IONIC POLYMER ACTUATORS

Curt S. Kothera and Donald J. Leo

Virginia Tech, Center for Intelligent Material Systems and Structures, Blacksburg, VA 24061

Abstract

Ionic polymer transducers exhibit coupling between the electrical, chemical, and mechanical domains, allowing their use as both sensors and actuators. Because of their compliance, light weight, and low voltage operation, ionic polymers have received considerable attention, although their fundamental mechanisms are still open for debate. While most of the existing models provide linear, dynamic approximations of the response, nonlinear characteristics have been observed in the laboratory. Recent experimental results have shown that the solvent plays a significant role in the dynamic response of these actuators in the cantilever configuration. Given a single-frequency input voltage, the major difference from changing solvents was concluded to be a varying distortion, seen in both the actuation current and tip velocity measurements. This research looks to further explore this nonlinear distortion by incorporating a larger set of candidate solvent materials and investigating the impact of how changing properties affect the overall response. System identification techniques using the Volterra series are employed to aid in the characterization of the harmonic distortion. The knowledge gained in this study will provide useful information about the nature of the nonlinearity and some of the factors that affect its relative influence, which will assist physical model development.

Introduction

Ionic polymers are a class of smart materials capable of producing large strain ($>1\%$) under the application of an electric field. The actuation phenomenon of this material and its sensing capability were independently discovered just over a decade ago.^{1,2} Several models have been proposed, but because the transduction properties were only recently discovered, a universally accepted model that fully accounts for all the dynamics does not yet exist. Part of the reason for this is that models developed from different principles are able to match simulation results to experimental data. One of the leading discrepancies comes about over the dominant mechanisms involved in the actuation response. A micromechanical model has been derived to conclude that electrostatic interaction dominates the step response,³ while a model developed using irreversible thermodynamics states that hydration and solvent motion are most domi-

nant.⁴ However, a common theme among these proposed models is the existence of thin activation layers near the electrodes, where the dominant mechanisms occur. In addition to the aforementioned models, other researchers have also arrived at this conclusion.⁵⁻⁸

While the development of a comprehensive model is still ongoing, there are some aspects that have received less attention. These include the dynamic response and nonlinearities. Nearly all of the proposed models focus on the quasi-static case of the step response, and either restrict or simplify their derivations to linear approximations. However, nonlinearities have been observed in the step response, including the introduction of permanent strain⁹ or remnant deformation¹⁰ in the polymer and effects from material dehydration.¹¹ Harmonic generation in the tip displacement and nonlinearities between charge and input voltage have also been observed experimentally. That being said, there have been a couple instances where nonlinear models of ionic polymers were developed. Nonlinear identification using a Hammerstein model has led to successful model development with ionic polymer materials in application to walking robots,¹² and work has also been conducted showing that the Volterra series offers an effective means to model the distortion in the response of ionic polymer actuators to harmonic inputs.¹³

The goal of this work is to experimentally characterize the nonlinearity seen in the actuation response of cantilever ionic polymer benders. Gaining more understanding of the mechanisms involved in the actuation response will aid in making ionic polymers viable transducer materials for use with flexible structures. Ionic polymers employing different solvents will be used for comparison. The first sample will contain water, which has been the most widely used solvent, despite the fact that it is volatile in air, making the material prone to dehydration. Ionic liquids will be used for the second and third samples. Ionic liquids are novel solvents that are gaining ground in electroactive polymer research because they offer a broadened electrochemical stability window and do not suffer from dehydration in open-air environments.¹⁴⁻¹⁶ It is expected that using solvents with such different properties will highlight differences in the nonlinear distortion. In particular, the viscosity of the three solvents spans two orders of magnitude.

The general analysis methodology will be detailed in the next section, followed by results from a preliminary study to be used as motivation. Experimental results of the nonlinear characterization will then be given, and the paper will end with a summary and conclusions.

Analysis Technique

This work looks to expand the idea of using the Volterra series to identify the nonlinear distortion observed in input-output measurements of ionic polymers.¹³ The actuator system is assumed to have the form of two single-input, single-output subsystems connected in series. The first subsystem represents the electrochemical processes with voltage as the input and current as the output, while the chemomechanical processes are represented by the second subsystem with current as the input and linear tip velocity as the output. By isolating the electrical and mechanical characteristics with this model structure, it was believed that insight of where the nonlinearity enters into the response could be determined. The system could actually have been described by a variety of different input-output relationships, but recent results conclude that the current (charge) is more correlated to the strain than the voltage,^{15,17} making this form reasonable.

The response of each system is analyzed independently using the Volterra series to separate the linear and nonlinear components in the signals, as shown in Figure 1. The discrete-time form of the Volterra series implemented here can be written as

$$y(k) = y_0 + \sum_{i=0}^m h_1(i)x(k-i)\Delta t + \sum_{i=0}^m \sum_{j=0}^m h_2(i,j)x(k-i)x(k-j)\Delta t^2 + \dots \quad (1)$$

where $y(k)$ is the output, $x(k)$ is the input, $h_n(\cdot)$ are the volterra kernels of degree n , and m is the order, or number of memory terms, used in the expansion. An advantage to this formulation is that the system response under consideration can be decomposed into individual components of various degrees¹⁸

$$y(t) = y_{linear}(t) + y_{quadratic}(t) + y_{cubic}(t) + \dots \quad (2)$$

where the output $y(t)$ is composed of terms of different powers, or degrees, of the input; stated more precisely, $y(t) = f(x(t), x^2(t), x^3(t), \dots, x^n(t))$. This concept of nonlinear component separation is used in

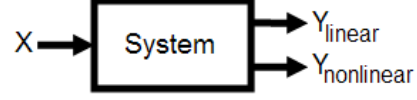


Figure 1. System structure used for nonlinear analysis.

the identification procedure, where all degrees of $n = 2$ and higher are lumped together, as in Figure 1.

The analysis methodology follows directly from above, where the output of each subsystem is composed of a linear and nonlinear portion

$$\tilde{Y} = \tilde{Y}_L + \tilde{Y}_N. \quad (3)$$

Here the *tilde* signifies data, the subscript L denotes the linear portion, and the subscript N denotes the nonlinear portion. When a single-tone sine wave is the input to a linear system, the Volterra expansion to represent the output has degree $n = 1$ and order $m = 2$. In relation to the polymer sample under consideration here, these are the values used to parameterize the linear model for analyzing the first subsystem (voltage-to-current). However, the same could not be used for the second subsystem because the input (current) may have already been distorted in the first subsystem. Treating this signal as the known input to the current-to-velocity subsystem, the linear output will have content at each of the frequencies contained in the current signal. Therefore, the power spectrum was used to determine the necessary order (twice the number of frequencies) for the linear output.

Once the linear portion of the signals was known, the nonlinear portion was calculated as the difference between the measured signal and the linear Volterra model

$$\begin{aligned} \tilde{Y}_N &= \tilde{Y} - Y_L \\ &= \tilde{Y} - h_{m_l}^{n_l}(\tilde{X}), \end{aligned} \quad (4)$$

where the subscript l on the order and degree indicates the expansion of the linear Volterra model. This nonlinear error signal is then used in the calculation of several Volterra models of varying order and degree to find the minimum-parameter model. The models are parameterized with a prediction data set and their quality is assessed by simulating their response to different data that will be called the validation data set. In determining the best model for the nonlinear component, both the prediction and validation data sets are checked. Different data is used to determine the best model because the measurement signals will likely contain some level of noise. This noise can create problems when parameterizing

a Volterra model as the order and degree increase. The calculation of the model parameters will work to actually fit the noise, requiring a high order and degree to get the prediction error to converge to zero, or near zero. If noise is in one or both measurements, the error will converge to some nonzero value that is proportional to the amount of noise in the signals. This noise-fitting that occurs in the prediction model will lead to poor validation results, assuming the noise is random, by creating an overly sensitive model. Since the model would match the noise in the prediction data, if the noise in the validation data differed at all, as it would, the validation error could be very large. This is why the concept of finding the “minimum-parameter” model comes up. A minimum-parameter model will fit only the general trend of a signal, leaving the error convergence value in the validation data to reflect the noise level.

With selection of the model parameters of the nonlinear component, this model can now be combined with the linear component to give the total model response

$$Y = h_{m_i}^{n_i}(\tilde{X}) + h_{m_o}^{n_o}(\tilde{X}), \quad (5)$$

where the subscript o on the order and degree of the nonlinear component refer to the minimum-parameter model. Now that full model has been identified, the amount of nonlinearity is then determined by comparing the model error of the full model to that of the linear model. This shows how the addition of nonlinear terms affects the error of the output predicted by the Volterra models. A preliminary study showing the utility of this analysis methodology will be discussed in the next section.

Preliminary Results

As a motivating example for studying the effect that different solvents have on the actuation response of ionic polymers, samples in two different forms were studied. Each sample has Nafion[®]-117 as the base ionomer, sodium as the cation, and platinum-gold electrodes.¹⁹ The difference between the samples is that the first sample has water as the solvent, while the second sample has been solvated with the ionic liquid 1-ethyl-3-methylimidazolium trifluoromethanesulfonate (EMI-Tf). While differing in dimensions, they do maintain a 4:1 length-to-width ratio (water: 8x2mm; EMI-Tf: 16x4mm). Sine wave experiments measuring the applied voltage, actuation current, and linear tip velocity were carried out and are reported for the test condition of 1.5V and 5.0Hz. Linear and nonlinear Volterra models were calculated at this test setting and compared to determine how much nonlinearity is contained in each response. A

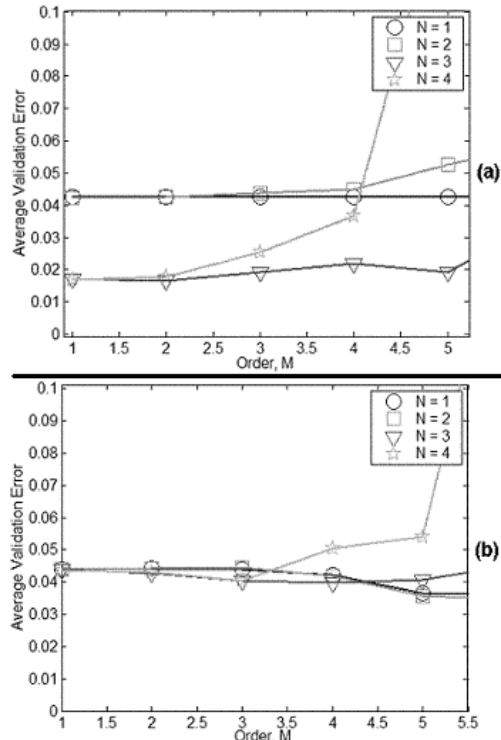


Figure 2. Validation error plots at 1.5V and 5.0Hz: (a) water sample; (b) EMI-Tf sample.

more detailed account of these voltage-controlled experiments and their results can be found.²⁰

Figure 2a shows the validation error plots for the water sample and Figure 2b shows the same for the ionic liquid sample. An interesting result is noticed by comparing these figures. It can be seen in Figure 2a that the error of the degree 1 and 2 models is consistently higher than that of the degree 3 and 4 models until higher order models become too sensitive. This indicates that the nonlinearity here is higher than second degree. When looking at Figure 2b, the same trend is not evident, possibly an indication that the response of the ionic liquid sample is predominantly linear at these conditions. It should also be noted that the minimum-parameter Volterra models ($h_m^n(\cdot)$) for this case is $h_2^3(\cdot)$ for the water sample and $h_4^3(\cdot)$ for the ionic liquid sample.

In examining the time response for this test condition, a similar conclusion can be drawn. Figure 3a has the results for one cycle of the water sample and Figure 3b shows the results for the ionic liquid. In these plots, the left and right columns of plots refer to prediction and validation results, respectively. The top row of plots show the linear model fit to the output data, the middle two plots show the nonlinear component (linear model error) and the Volterra out-

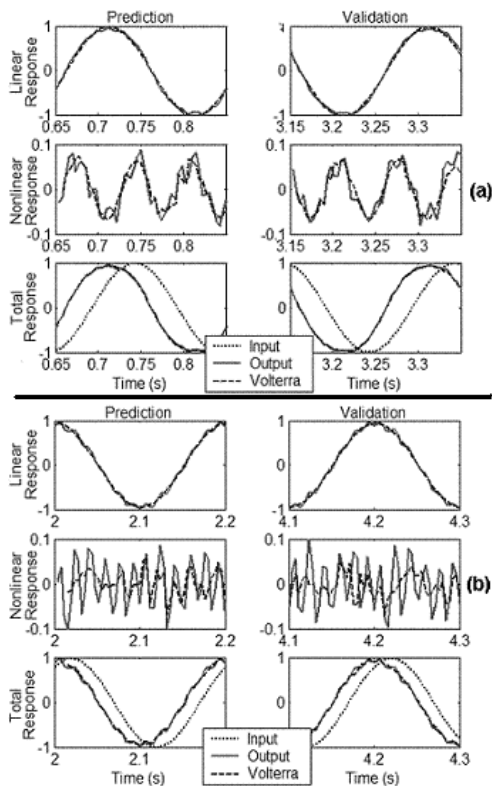


Figure 3. Time response plots at 1.5V and 5.0Hz: (a) water sample; (b) EMI-Tf sample.

put for it, and the bottom plots show the combined response along with the input. In this figure, the dotted line is the input signal (voltage), the solid line is the output signal (current), and the dashed line is the noted Volterra model output. Comparing the linear and nonlinear components to one another and to the measured current signal in Figure 3a, it does appear that the nonlinearity is a cubic mechanism since the nonlinear component goes through three cycles in the time it takes the linear component and input to go through one. On the contrary, there seems to be no discernible trend for the ionic liquid sample in Figure 3b. However, one thing to note with the ionic liquid sample is that it draws much less current (approximately an order of magnitude lower) than the water sample. This leads to higher noise levels in the current measurement of this sample, as can be seen in the plots of Figure 3b, but a more elaborate current sensing system would be required to produce better results.

Overall, the addition of the nonlinear model to the water sample reduces the output error from 4.3% to 1.7%, while adding nonlinear terms to the model of the ionic liquid sample gives no further reduction from the initial 4.0% error with the linear model.

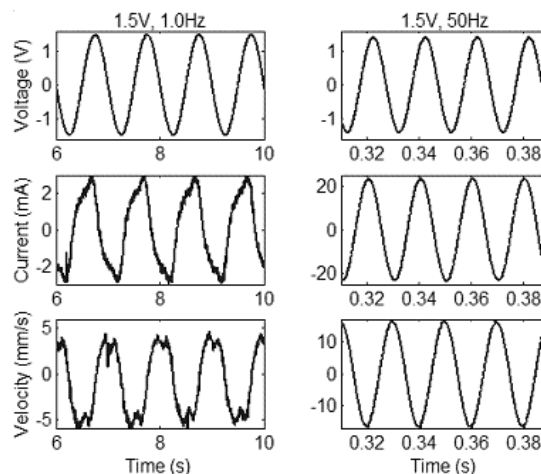


Figure 4. Actuation response of water sample at different frequencies.

Since two subsystems are included in the actuator system model, it should be noted that the current-to-velocity subsystem results were similar to one another for each of the samples, and it was the voltage-to-current subsystem that highlighted the effects from changing the solvent material. This gives evidence that the electrical characteristics add more nonlinearity into the overall response of the system.

Another interesting finding was that when investigating the response at different frequencies for the water sample, different levels of distortion were visually apparent. This is shown in Figure 4 for 1.5V amplitude sine waves. On the left side are measurements at 1.0Hz and results at 50Hz are shown on the right. The figure shows that, in addition to solvent-induced nonlinearity discussed above, the influence of the nonlinearity also seems to have frequency dependence. This will be explored further in the following investigation.

Frequency-dependence Investigation of Nonlinearity

This section will focus in on the frequency dependence of the nonlinearity that was shown in the preliminary results. With the intent of producing more directly comparable results, some modifications will be made to the analysis procedure. As it was noted before, the signal-to-noise ratio for the current signal of the ionic liquid sample was an order of magnitude lower than that for the water sample, which could affect the results. Due to limitations of the current sensing circuit used for the preliminary results, a transconductance amplifier was constructed and used for the results to follow. This amplifier takes in a voltage waveform and produces a current signal of the same shape and proportional amplitude,

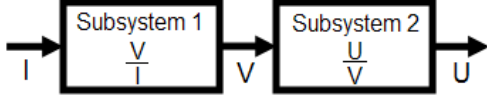


Figure 5. Modified system decomposition.

allowing for a known current to be supplied to the polymer and eliminating the poor sensor resolution problem. The assumed structure of the model will be modified with this adjustment. With current as the new input to the polymer system, the electrochemical subsystem will be reversed from voltage-to-current to current-to-velocity (I-V). Additionally, the linear tip displacement of the cantilever samples will be used as the system output because the displacement measurements tend to be better than velocity at low frequencies. This means that the second subsystem has also been changed from current-to-velocity to voltage-to-displacement (V-U). Figure 5 has been included to show the new system. For this new system description, subsystem 1 is the electrical impedance and subsystem 2 is essentially the strain per unit volt.

Laboratory Setup

To conduct an experimental investigation using the described analysis procedure, data from three polymer samples was collected. Each sample uses the commercially available Nafion[®]-117 as the base ionomer and lithium as the cation. The first sample, which will henceforth be referred to as Sample 1, uses deionized water as the solvent and measures (20x2x0.2)mm. The platinum portion of the electrodes is chemically deposited with a thin gold layer electro-plated over it. It was prepared using an impregnation/reduction method.¹⁹ The second sample (Sample 2) uses the ionic liquid 1-ethyl-3-methylimidazolium trifluoromethanesulfonate (EMI-Tf) as the solvent, and Sample 3 is solvated with the ionic liquid 1-butyl-1-methyl-pyrrolidinium tris(pentafluoroethyl)trifluorophosphate (BMPyr-tris). The viscosity of EMI-Tf is 45cP and that of BMPyr-tris is 224cP. Noting that water has a viscosity of 1.0cP, this range spans two orders of magnitude. Each ionic liquid sample also measures (30x3x0.3)mm, which is different than Sample 1, but since they maintain the 10:1 length-to-width ratio, it is believed that they will not adversely affect any conclusions. The electrodes of samples 2 and 3 have a layer of platinum applied as in Sample 1, but the gold layer is hot pressed on. It should be noted that the water sample will not tolerate the hot pressing procedure, but since water samples prepared as Sample 1 are the most common to date, it was fabricated more as a baseline case. Table 1

Table 1. Summary of Actuator Compositions.

Actuator Component	Sample 1	Sample 2	Sample 3
Ionomer	Nafion [®]	Nafion [®]	Nafion [®]
Cation	Li ⁺	Li ⁺	Li ⁺
Electrode	Pt - Au	Pt - Au	Pt - Au
Solvent	H ₂ O	EMI-Tf	BMPyr-tris
Viscosity (cP)	1	45	224

summarizes the composition of each actuator, where it is seen that the solvent is the only difference.

In these experiments, voltage, current, and displacement were measured. For data acquisition, a dSPACE DS2003 analog-to-digital converter and DS 2103 digital-to-analog converter were used. The A/D converters had a 16-bit range and were set to $\pm 5.0V$ for Samples 1 and 2, and $\pm 10.0V$ for Sample 3 because of higher impedance levels. A laser vibrometer (Polytec OFV 3001 Controller and 303 Sensor Head) was used to measure the tip velocity and displacement of the cantilever ionic polymer actuators. The sensitivity was adjusted from test to test depending on the signal characteristics to ensure that the A/D range was used as effectively as possible. The input signal was generated by the dSPACE system and passed through a transconductance amplifier to get an input current. The voltage data collection occurred at the output of the amplifier. Finally, to hold the cantilever polymer and apply the electric field, a test fixture with gold foil electrodes was used. Figure 6 has been included to show the necessary equipment, along with the measured voltage (V), current (I), and velocity/displacement (U) signals.

Two sets of experiments were run with these three samples. The first are single-frequency sine wave tests, scaled in frequency based on the mechanical resonance of the first bending mode and occurring at multiples of this resonance frequency of 1, 0.75, 0.5, 0.25, and 0.1. The amplitudes varied across the samples since the impedance plays a part in the voltage measurement. The sample rate was also varied from test to test, but was kept a constant multiple of the actuation frequency over the frequency range, which provided the same number of points per cycle in each test. Setting this multiple to 200 allowed full use of the sample rate range in the data acquisition system. For the second set of tests, frequency response functions were captured for each subsystem. The input was a mean-zero Gaussian signal with various root-mean-square (RMS) levels, depending on the im-

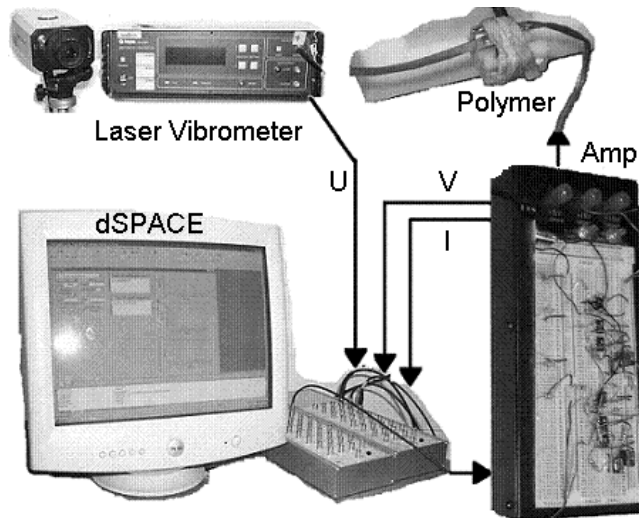


Figure 6. Experimental setup for ionic polymer actuator testing.

pedance of each sample, and band-limited based on the mechanical resonance. For the ionic liquid samples, 15 data sequences were averaged, but only 5 were averaged for the water sample. This is because the water sample dehydrates in an open-air environment and the testing time was kept below one minute to avoid any potentially skewed results.

Single Frequency Results

Here the results from the single frequency sine waves experiments will be discussed. Because plotted results were shown in the preliminary results section, and because of the large number of results (15 test conditions per sample), they will be omitted here. Instead the results for each of the test conditions will be reported in tabular form for each sample. Tables 2, 3, and 4 show the Volterra modeling results for samples 1, 2, and 3, respectively. In these tables the amplitudes are ordered highest to lowest from top to bottom and the frequencies appear lowest to highest from left to right. Each cell of results displays the average linear Volterra model error first and the average nonlinear Volterra model error last, separated by the minimum-parameter nonlinear model form in parentheses (h_m^n). To determine the effect of adding nonlinear terms to each model, the linear error can be compared to the nonlinear error. For instance, in the first cell of Table 2 (8.0mA, 1.68Hz), the linear model error of 6.6% is reduced to only 2.9% by adding a nonlinear Volterra model of order $m = 4$ and degree $n = 3$. Looking at all the results, it can be seen that some of the Sample 3 results for the V-U subsystem appear to have unusually large errors. It

should be noted that this is caused by low signal levels and drift in the displacement measurement, not poor model construction.

In comparing the results for each of the actuator samples, the most consistent trend that can be seen is related to the electrical characteristics (subsystem 1). That is, as the viscosity in the samples increases, the linear Volterra model error between the input current and output voltage decreases. This means that with larger linear model error, the samples with lower viscosity benefit more from nonlinear model terms in more accurately predicting the measured voltage with the given current signal. Figure 7 shows these results for the three samples. The top plot shows the linear error for Sample 1 (1.0cP), the middle plot shows the error for Sample 2 (45cP), and the bottom plot shows the results for the most viscous solvent, Sample 3, at 224cP. In this figure the vertical axis is the average linear model error percentage and the horizontal axis has the normalized frequencies. The frequencies were normalized with respect to the mechanical resonance for a more direct comparison, and the actual values can be found in the tables.

Another indication of this nonlinear effect is apparent when considering the degree of the Volterra models and the lack of an improved response prediction. For example, several of the model degrees for the I-V subsystem in Sample 3 achieved the best minimum-parameter results with just another linear model ($n = 1$), and the error is reduced very little with the addition of more terms to the model. When examining the results for Samples 1 and 2, the nonlinear Volterra models are nearly all of degree 3 for the electrical subsystem, showing much improvement when comparing the linear error to the nonlinear error. The fact that so many of the minimum-parameter Volterra models are third degree also provides more evidence that the nonlinear mechanism could be cubic.

Looking more closely at these results, there is also evidence that the nonlinearity could be amplitude dependent. This is more clearly seen in the bottom two plots of Figure 7, which correspond to the two ionic liquid samples. It appears that the linear error increases with the amplitude of the input current, implying that the voltage response becomes more distorted as the input level increases. Any trend relating the linear error to the actuation frequency is less apparent here, but the next set of results will show the frequency response.

Frequency Response Results

To investigate any nonlinearity in the actuation response of these materials over a larger number of

Table 2. Volterra model errors for Sample 1 (values in percent, %).

Amplitude (mA-rms)	Sub- system	Frequency (Hz)									
		1.68		4.19		8.37		12.56		16.75	
8.0	I-V	6.6 (h_4^3)	2.9	7.2 (h_5^3)	3.9	7.1 (h_6^3)	3.3	6.3 (h_6^3)	2.3	7.5 (h_4^3)	4.9
8.0	V-U	1.9 (h_4^3)	1.2	2.8 (h_5^3)	1.3	6.1 (h_5^3)	1.4	1.4 (h_6^3)	1.2	2.5 (h_6^3)	1.3
4.0	I-V	6.2 (h_5^3)	3.1	7.6 (h_5^3)	6.3	7.4 (h_5^3)	3.6	8.1 (h_4^3)	7.1	4.3 (h_6^3)	2.0
4.0	V-U	3.1 (h_3^3)	2.1	2.9 (h_6^3)	2.0	4.5 (h_5^3)	3.2	1.6 (h_2^3)	1.5	7.4 (h_5^3)	3.9
2.0	I-V	8.1 (h_4^3)	4.2	5.6 (h_6^3)	1.8	9.1 (h_6^2)	5.5	8.4 (h_6^2)	4.4	7.9 (h_5^3)	3.4
2.0	V-U	2.9 (h_2^3)	2.0	4.4 (h_4^2)	4.0	6.2 (h_8^1)	6.1	4.1 (h_4^1)	4.1	2.5 (h_3^3)	1.6

Table 3. Volterra model errors for Sample 2 (values in percent, %).

Amplitude (mA-rms)	Sub- system	Frequency (Hz)									
		1.10		2.75		5.50		8.25		11.0	
5.0	I-V	5.0 (h_7^3)	1.9	2.5 (h_7^3)	0.6	2.4 (h_6^3)	0.7	1.7 (h_8^2)	0.7	2.8 (h_4^3)	2.0
5.0	V-U	1.3 (h_6^3)	0.5	1.8 (h_2^2)	0.6	1.8 (h_3^3)	0.5	6.5 (h_8^2)	4.0	0.8 (h_8^1)	0.5
3.5	I-V	2.3 (h_4^3)	0.7	3.8 (h_3^3)	1.9	2.9 (h_7^2)	1.0	1.3 (h_8^1)	0.6	2.7 (h_7^2)	1.1
3.5	V-U	3.1 (h_5^3)	1.2	5.8 (h_3^3)	3.5	1.3 (h_2^3)	0.7	4.7 (h_4^3)	2.8	1.4 (h_8^1)	0.6
2.0	I-V	5.2 (h_7^2)	1.7	6.2 (h_4^3)	4.6	4.9 (h_5^3)	3.1	3.4 (h_8^1)	2.2	3.3 (h_5^3)	1.9
2.0	V-U	2.0 (h_2^3)	0.7	3.9 (h_7^2)	2.2	7.9 (h_8^2)	4.3	8.7 (h_3^3)	5.7	2.9 (h_5^3)	1.9

Table 4. Volterra model errors for Sample 3 (values in percent, %).

Amplitude (mA-rms)	Sub- system	Frequency (Hz)									
		1.2		3.0		6.0		9.0		12.0	
1.25	I-V	2.0 (h_4^3)	0.9	1.5 (h_5^3)	0.8	1.2 (h_8^1)	1.0	1.3 (h_8^1)	1.1	1.2 (h_2^2)	1.0
1.25	V-U	8.3 (h_2^3)	7.6	6.4 (h_8^1)	6.3	6.6 (h_8^1)	5.7	9.8 (h_4^1)	7.7	4.0 (h_4^2)	3.3
1.00	I-V	1.9 (h_8^2)	0.6	1.7 (h_5^3)	1.1	1.6 (h_8^1)	1.2	1.6 (h_3^3)	1.4	1.3 (h_3^3)	1.1
1.00	V-U	3.6 (h_3^3)	3.5	13.1 (h_4^3)	12.2	16.6 (h_2^2)	16.6	10.7 (h_8^1)	8.7	6.1 (h_2^3)	5.8
0.75	I-V	3.5 (h_5^3)	1.7	2.5 (h_5^3)	1.5	2.3 (h_4^1)	1.9	1.8 (h_8^1)	1.4	1.4 (h_2^3)	1.2
0.75	V-U	9.3 (h_4^3)	8.6	16.6 (h_3^3)	16.4	13.9 (h_8^1)	8.3	20.0 (h_8^2)	17.5	11.7 (h_3^4)	11.5

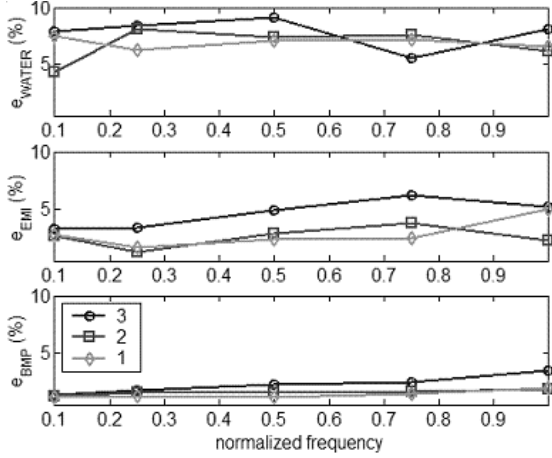


Figure 7. Linear Volterra model error of I-V subsystem.

frequencies, frequency response functions were measured. Figure 8a gives the subsystem 1 response, which is the electrical impedance, and Figure 8b shows the response of subsystem 2. In this plot the displacement has been converted to strain according to $\epsilon = ut/l^2$, where u is the displacement, t is the thickness, and l is the length of the cantilever actuator. This is an approximation assuming constant curvature, which is reasonable up to, and including, the first bending mode. Results from two different input levels are shown. The lower is 0.5mA-rms (dotted) and the higher is 2.5mA-rms (solid). Sample 1 is shown in light gray, Sample 2 is dark gray, and the Sample 3 curves are black, so the darker the line, the higher the viscosity of the solvent.

An indication of a nonlinear system is immediately observed by the magnitude scaling seen in both plots. Had the system been linear, an increase in the input would correspond to the same increase in the output, so the ratio would have remained constant. This is not the case here, however. Instead there is a consistent trend for all three samples that increasing the input current produces less voltage, decreasing the impedance, as seen in Figure 8a. This scaling appears to increase at low frequencies and vanish at high frequencies, where the impedance levels off. It also appears that actuators with higher viscosity solvents have an increased scaling over the same change in input RMS level. Figure 9a has been included to bring out this viscosity-related trend more clearly. In this figure the impedance magnitude ratios of low input to high input are plotted for all three samples, where it is seen that Sample 3 shows the least amount of scaling and Sample 1 has the most.

Interesting to note is that these frequency response results show, contrary to the sine wave results, that

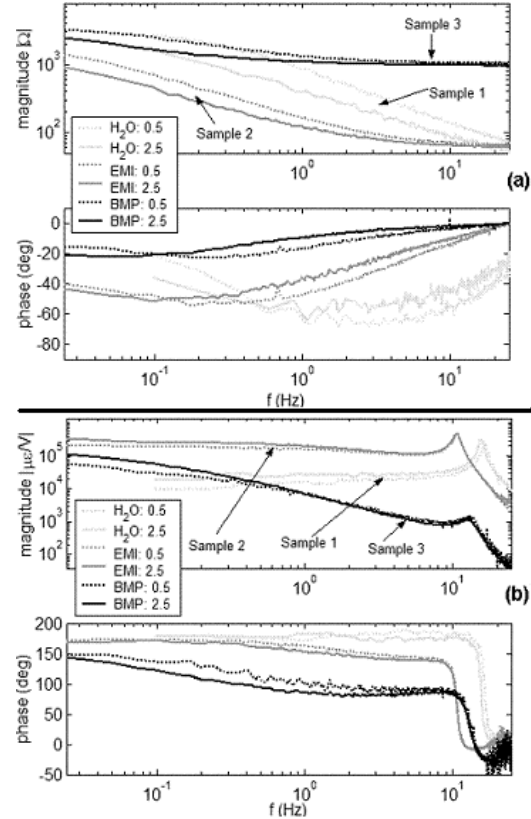


Figure 8. Frequency response functions for different levels of input current: (a) current-to-voltage; (b) voltage-to-strain.

the response of Sample 3 is nonlinear in the same frequency range, although the magnitude scaling is relatively small. Re-examining the numbers in Table 4, it can be seen by comparing the errors of the linear and nonlinear models that the addition of nonlinear terms has more impact on lowering the output error as the frequency decreases, which is consistent with the magnitude scaling trend seen in Figures 8a and 9a.

Turning attention now to the strain plot, Figure 8b, a decrease in the resonance frequency is noticed with increasing input amplitude, in addition to the magnitude scaling. It also appears that a lower viscosity solvent will give a larger shift for the same increase in input current. Figure 9b examines this shift more closely by plotting the strain ratio from low input to high input current. It is seen that the strain increase is higher in Sample 1 than Sample 2 (lower ratio), and Sample 3 actually shifts in the opposite direction since its ratio is greater than one. When taking into consideration the impedance results (more current produces less voltage), this can be translated into saying that lower voltages, which draw more current,

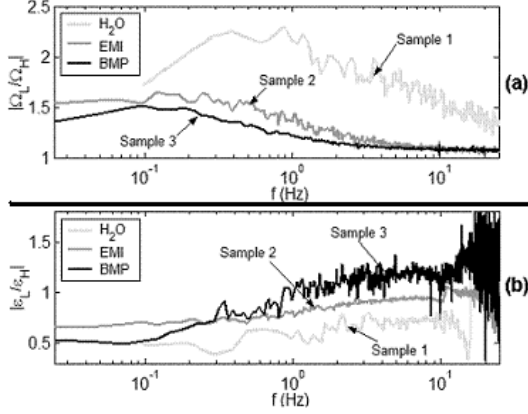


Figure 9. Magnitude ratios of low current to high current input: (a) current-to-voltage; (b) voltage-to-strain.

cause greater levels of strain in the range tested. Seeing that both in the preliminary results and in the single frequency results mentioned above there was evidence of a cubic nonlinearity, this decreasing resonance frequency and low frequency magnitude scaling could also add support to this nonlinear form. This statement is made in relation to the response of a single-degree-of-freedom system with a softening spring that behaves similarly to the results shown.

This apparent nonlinearity between voltage and strain could be slightly misleading when considering the actuator system as a whole, however. Under the assumed model structure with current as the input and displacement as the output, the voltage is an internal link between the electrical response and the mechanical response. The results in Figure 8a show that there is a nonlinear relationship between the current and voltage, so the nonlinear relationship seen between the voltage and strain could be, at least in part, a byproduct of this electrical nonlinear characteristic. When examining the single-input, single-output frequency response function of the complete actuator system (current-to-strain), Figure 10 shows that the low frequency magnitude scaling is less evident, but the shifting resonance can still be seen. Additionally, these results show that the magnitude near resonance is now scaled differently than in Figure 8b, with less motion resulting from higher current. This indicates a nonlinear relationship between current and strain, as well.

Conclusions

Both single frequency sinusoids and frequency response functions were used to experimentally characterize the nonlinear response of cantilever ionic polymer actuators in three different solvent forms.

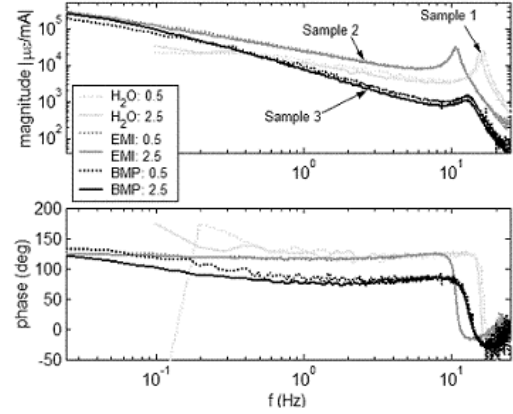


Figure 10. Frequency response functions of overall system for different levels of input current.

Nonlinear Volterra modeling of the harmonic excitations to the assumed system form of two serially connected single-input single-output subsystems was carried out, and results provide evidence that the electrical response for higher viscosity solvents, such as BMPyr-tris, is predominantly linear, while lower viscosity solvents, such as water and EMI-Tf, require nonlinear input-output relationships to assure low model prediction error. Frequency response measurements confirmed the nonlinearity between current and voltage by showing that increased current results in lower voltage, and that higher viscosity solvents cause less impedance magnitude scaling at low frequencies. Additionally, the nonlinearity in the mechanical response showed that the resonance frequency decreased as the input increased, much like a softening (cubic) spring system, and that the strain magnitude scaling reversed depending on whether current or voltage was considered as input. Being that each of the input-output relationships for the two subsystems and the overall system contain nonlinearity, it can be concluded that a more effective model may allow the current and the voltage to directly influence the bending response of these ionic polymer actuators. As such, future work will explore the validity of different system structures, including parallel-interconnected subsystems that allow both the current and the voltage to contribute to the mechanical deformation.

Acknowledgements

The authors would like to thank the National Science Foundation and the Virginia Space Grant Consortium for funding. The authors greatly acknowledge the support.

References

1. K. Oguro, Y. Kawami, and H. Takenaka, "Bending of an ion-conducting polymer film-electrode composite by an electric stimulus at low voltage," *Trans. Journal of Micromachine Society* **5**, pp. 27–30, 1992.
2. K. Sadeghipour, R. Salomon, and S. Neogi, "Development of a novel electrochemically active membrane and 'smart' material based vibration sensor/damper," *Smart Materials and Structures* **1**, pp. 172–179, 1992.
3. S. Nemat-Nasser, "Micromechanics of actuation of ionic polymer-metal composites," *Journal of Applied Physics* **92**(5), pp. 2899–2915, 2002.
4. P. deGennes, K. Okumura, M. Shahinpoor, and K. Kim, "Mechanoelectric effects in ionic gels," *Europhysics Letters* **50**(4), pp. 513–518, 2000.
5. K. Asaka and K. Oguro, "Bending of polyelectrolyte membrane platinum composites by electric stimuli, part ii. response kinetics," *Journal of Electroanalytical Chemistry* **480**, pp. 186–198, 2000.
6. S. Tadokoro, S. Yamagami, T. Takamori, and K. Oguro, "An actuator model of icpf for robotic applications on the basis of physicochemical hypotheses," in *IEEE International Conference on Robotics and Automation*, **2**, pp. 1340–1346, (San Francisco, CA), April 2000.
7. Y. Xiao and K. Bhattacharya, "Modeling electromechanical properties of ionic polymers," in *SPIE Smart Materials Conference*, **4329**, pp. 292–300, 2001.
8. K. Farinholt and D. Leo, "Modeling of electromechanical charge sensing in ionic polymer transducers," *Mechanics of Materials* **36**(5-6), pp. 421–433, 2004.
9. K. Newbury and D. Leo, "Electromechanical modeling and characterization of ionic polymer benders," *Journal of Intelligent Material Systems and Structures* **13**(1), pp. 51–60, 2002.
10. Y. Bar-Cohen, X. Bao, S. Sherrit, and S.-S. Lih, "Characterization of the electromechanical properties of ionomeric polymer-metal composite (ipmc)," in *SPIE Smart Materials Conference*, **4695**, pp. 286–293, 2002.
11. C. Kothera, D. Leo, and L. Robertson, "Hydration and control assessment of ionic polymer actuators," in *AIAA Structures, Structural Dynamics, and Materials Conference*, (Norfolk, VA), April 2003.
12. M. Yamakita, N. Kamanichi, Y. Kaneda, K. Asaka, and Z.-W. Luo, "Development of artificial muscle actuator using ionic polymer with its application to biped walking robots," in *SPIE Smart Materials Conference*, **5051**, pp. 301–308, 2003.
13. C. Kothera, S. Lacy, R. Erwin, and D. Leo, "Nonlinear identification of ionic polymer actuator systems," in *SPIE Smart Materials Conference*, **5383**, (San Diego, CA), March 2004.
14. W. Lu, A. Fadeev, B. Qi, E. Smela, B. Mattes, J. Ding, G. Spinks, J. Mazurkiewicz, D. Zhou, G. Wallace, D. MacFarlane, S. Forsyth, and M. Forsyth, "Use of ionic liquids for pi-conjugated polymer electrochemical devices," *Science* **297**, pp. 983–987, 2002.
15. B. Akle, M. Hickner, D. Leo, and J. McGrath, "Electroactive polymers based on novel ionomers," in *ASME International Mechanical Engineering Congress*, (Washington, D.C.), November 2003.
16. M. Bennett and D. Leo, "Ionic liquids as stable solvents for ionic polymer transducers," *Sensors and Actuators A: Physical* **115**(1), pp. 79–90, 2004.
17. B. Akle and D. Leo, "On the relationship between the electric double layer and actuation in ionomeric polymer transducers," in *Material Research Society (MRS) Fall Meeting*, **95478**, (Boston, MA), November 2004.
18. P. Eykhoff, *System Identification: Parameter and State Estimation*, Wiley-Interscience, John Wiley and Sons Inc., London, 1974.
19. M. Bennett and D. Leo, "Manufacture and characterization of ionic polymer transducers employing non-precious metal electrodes," *Smart Materials and Structures* **12**(3), pp. 424–436, 2003.
20. C. Kothera and D. Leo, "Identification of the nonlinear response of ionic polymer actuators using the volterra series," *Journal of Vibration and Control (in press)*, 2005.